communications earth & environment

Article

https://doi.org/10.1038/s43247-024-01411-w

Deep seafloor hydrothermal vent communities buried by volcanic ash from the 2022 Hunga eruption

Roxanne A. Beinart[1,12] ✉, Shawn M. Arellano[2,3,4,12], Marcus Chaknova[5,6,7], Jasper Meagher[1], Andrew J. Davies[1,8], Joseph Lopresti[1], Emily J. Cowell[9], Melissa Betters[9], Tanika M. Ladd[2], Caitlin Q. Plowman[5,6], Lauren N. Rice[5,6], Dexter Davis[2], Maia Heffernan[4], Vanessa Jimenez[1,2,3], Tessa Beaver[2,3], Johann Becker[10], Sebastien Bergen[5,6], Livia Brunner[11], Avery Calhoun[5,6], Michelle Hauer[1], Aubrey Taradash[5,6], Thomas Giachetti[7] & Craig M. Young[5,6]

Mass mortality of marine animals due to volcanic ash deposition is present in the fossil record but has rarely been documented in real time. Here, using remotely-operated vehicle video footage and analysis of ash collected at the seafloor, we describe the devastating effect of the record-breaking 2022 Hunga submarine volcanic eruption on endangered and vulnerable snail and mussel species that previously thrived at nearby deep-sea hydrothermal vents. In contrast to grazing, scavenging, filter-feeding, and predatory vent taxa, we observed mass mortality, likely due to smothering during burial by thick ash deposits, of the foundation species, which rely on symbiotic chemosynthetic bacteria for the bulk of their nutrition. This is important for our broad understanding of the natural disturbance of marine ecosystems by volcanic eruptions and for predicting the effects of anthropogenic disturbance, like deep-sea mining, on these unique seafloor habitats.

Rapid deposition of volcanic tephra following an eruption can cause mass mortality of animal communities[1], though, in the ocean, this has been observed only rarely, even in shallow habitats[2–7]. Fossilized aggregations of marine animals in volcaniclastic sediment and ash are exceptionally well-preserved, providing historical evidence for the significance of these events and subsequent shifts in faunal community composition[8–18]. However, the paucity of modern observations of the effects of ash fall on marine communities means that we do not have the depth of understanding regarding ecosystem or organismal response, resilience, and succession after volcanic eruptions that we have for terrestrial ecosystems[1].

Eruptive activity at the Hunga volcano (previously called the Hunga TongaHunga Ha'apai volcano), Kingdom of Tonga, began on December 20, 2021, ending with a record-breaking explosive eruption that sent a plume of material as high as 58 km on January 15, 2022[19,20]. Additionally, up to 10 km^3 of the seafloor was displaced from the caldera walls and flanks via submarine density currents (SDC) during this eruptive period, with major impacts on the seafloor as far as 80 km from the caldera[21,22]. Approximately 3 months later (April 2022), we conducted a series of remotely operated vehicle (ROV) dives at five active hydrothermal vent fields and one inactive field along the Eastern Lau Spreading Center-Valu Fa Ridge in the Lau back-arc basin. These ranged in distance from 83 to 222 km west of the Hunga caldera (Fig. 1, Table S1). Our expedition provided a unique opportunity to explore the impact of volcanic activity on deep-sea marine ecosystems and to study community recovery and succession following a major volcanic event of unprecedented magnitude.

[1]Graduate School of Oceanography, University of Rhode Island, Narragansett, RI, USA. [2]Shannon Point Marine Center, Western Washington University, Anacortes, WA, USA. [3]Biology Department, Western Washington University, Bellingham, WA, USA. [4]Marine and Coastal Science Program, Western Washington University, Bellingham, WA, USA. [5]Oregon Institute of Marine Biology, University of Oregon, Charleston, OR, USA. [6]Department of Biology, University of Oregon, Eugene, OR, USA. [7]Department of Earth Sciences, University of Oregon, Eugene, OR, USA. [8]Department of Biological Sciences, University of Rhode Island, Kingston, RI, USA. [9]Department of Biology, Temple University, Philadelphia, PA, USA. [10]Department of Ocean Engineering, University of Rhode Island, Narragansett, RI, USA. [11]Department of Ocean Systems, Royal Netherlands Institute for Sea Research, Texel, Netherlands. [12]These authors contributed equally: Roxanne A. Beinart, Shawn M. Arellano. ✉e-mail: rbeinart@uri.edu

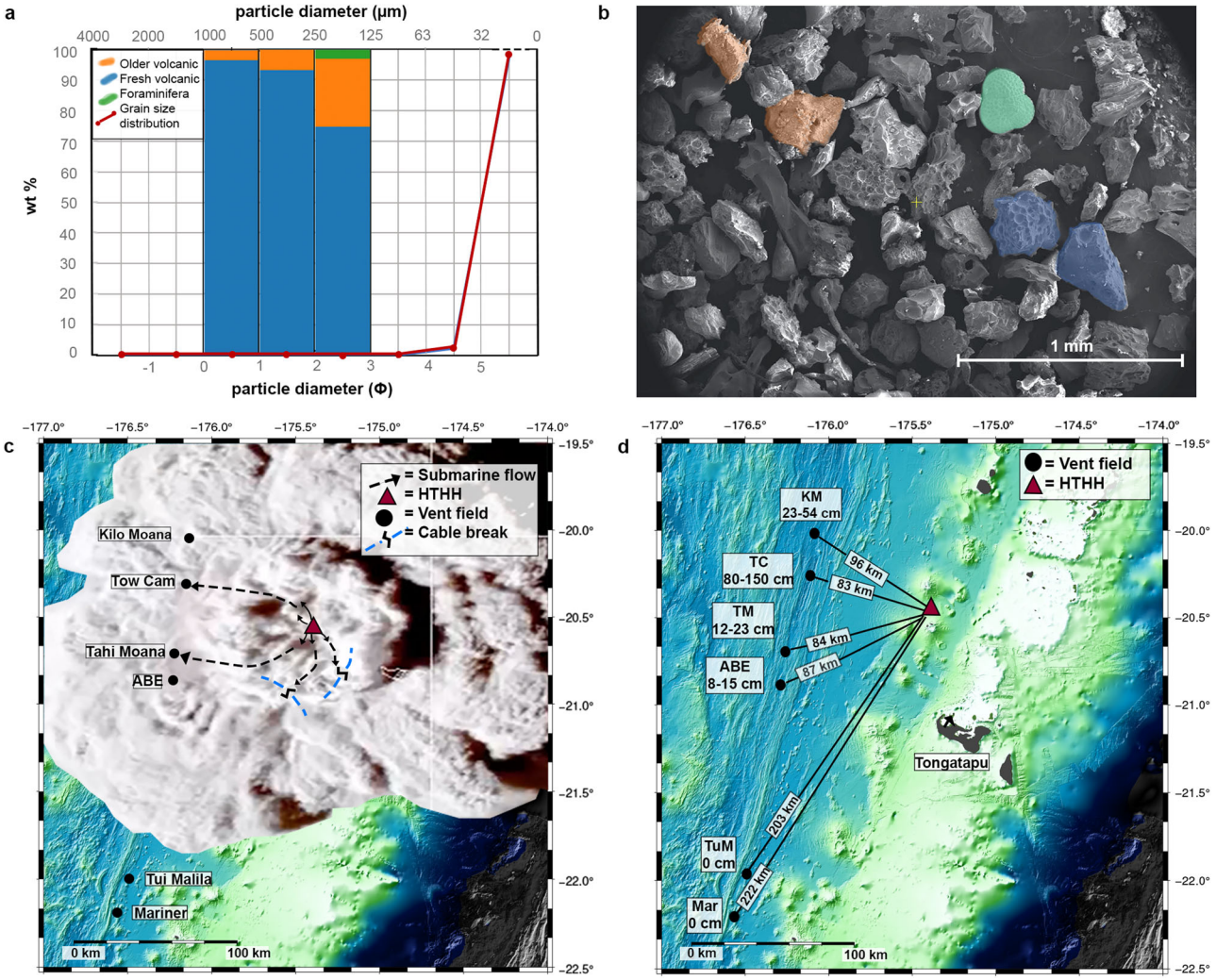

Fig. 1 | Thickness, possible modes of arrival, and componentry of Hunga volcanic ash found at the Eastern Lau Spreading Center—Valu Fa Ridge hydrothermal vents. a Componentry (colored vertical bars) of grains clearly discernable under stereomicroscope (>125 μm) and grain size distribution (red line) of ash collected from Tow Cam. **b** Scanning electron micrograph of bulk ash sample from Tow Cam. Particle color corresponds to examples of the particle categories selected for in componentry: older volcanic (orange), fresh volcanic (blue), foraminifera (green). **c** Plume imagery at 4:46 UTC on January 15, 2022 provided by Himawari from the Data Integration and Analysis System (DIAS) by Japan Agency for Marine-Earth Science and Technology (JAMSTEC). Predicted submarine flow routes based on ash deposit thickness, and particle properties. **d** Bathymetry of sample sites made with the Generic Mapping Tools v6[81], their corresponding distance from the Hunga volcano, and ash deposit thickness. Vent field abbreviations are as follows: KM Kilo Moana, TC Tow Cam, TM Tahi Moana, TuM Tu'i Malila, Mar Mariner.

Results and discussion

Thick ash deposits from the Hunga Volcano observed at deep-sea hydrothermal vents

Here, we report the first observations of ash deposition from the Hunga submarine volcano at nearby deep-sea hydrothermal vents. Our ROV dives revealed a north-to-south gradient in ash sedimentation thickness, with the thickest deposits in the northern vent fields and no apparent deposits at the most southern vent fields (Fig. 1, Table S2). These vent fields have been observed many times, most recently in 2019 during the CHUBACARC expedition[23], and were not previously sedimented (Fig. 2)[24]. We recovered over 25 kg of sediment material by scoop from deposits ranging in thickness from 7 to 150 cm (Tables S2 and S3). The thickest deposits were from Tow Cam (80–150 cm) (Fig. 1, Table S2), the vent field nearest to the Hunga volcano. The material collected was extremely fine-grained volcanic ash (89–99 wt% <63 μm) (Figs. 1, S1–S3). Grain size distribution was consistent at all vent fields with a mean particle diameter of 26–31 μm (Figs. 1 and S3). The deposits were rich in juvenile volcanic glass (>80% of point-counted grains) ranging from dense to pumiceous and contained 1–30% lithics (Figs. 1 and S3). We interpret this material to have come from the January 2022 eruption of the Hunga volcano. This interpretation is based on the immense deposit volume, very fine grain size distribution, and recent deposition on vent fields observed devoid of sediment during the 2019 CHUBACARC cruise[10] (Figs. 1 and S1–3).

The mode of ash deposition at these sites is still under question. Two hypotheses have emerged: subaerial fallout from the volcanic plume and/or submarine density current and consequential resuspension of fine particles (<2 mm). The initial ash-containing volcanic cloud centered on the Hunga Volcano had a maximum diameter of 260 km[25], encompassing the visited vent sites (Fig. 1). Ash fall was recorded for 10 h on the island of Tongatapu, Kingdom of Tonga, 65 km southeast of the Hunga caldera after the main eruption[25]. Given the particle size distribution observed to the west (89–99 wt% <63 μm) (Figs. 1 and S3), sinking rates would have allowed ash to fall from the ocean's surface to these seafloor vent fields (~1800–2800 m below the sea surface) within a few days to weeks by rapid vertical settling currents[26–28]. Settling of ash was observed in the water column two months following the eruption[29]. The Hunga eruption also produced massive submarine flows along the northwest and southeast flanks[21]. It is suspected that the flows transitioned into dilute SDCs that transported a large volume of

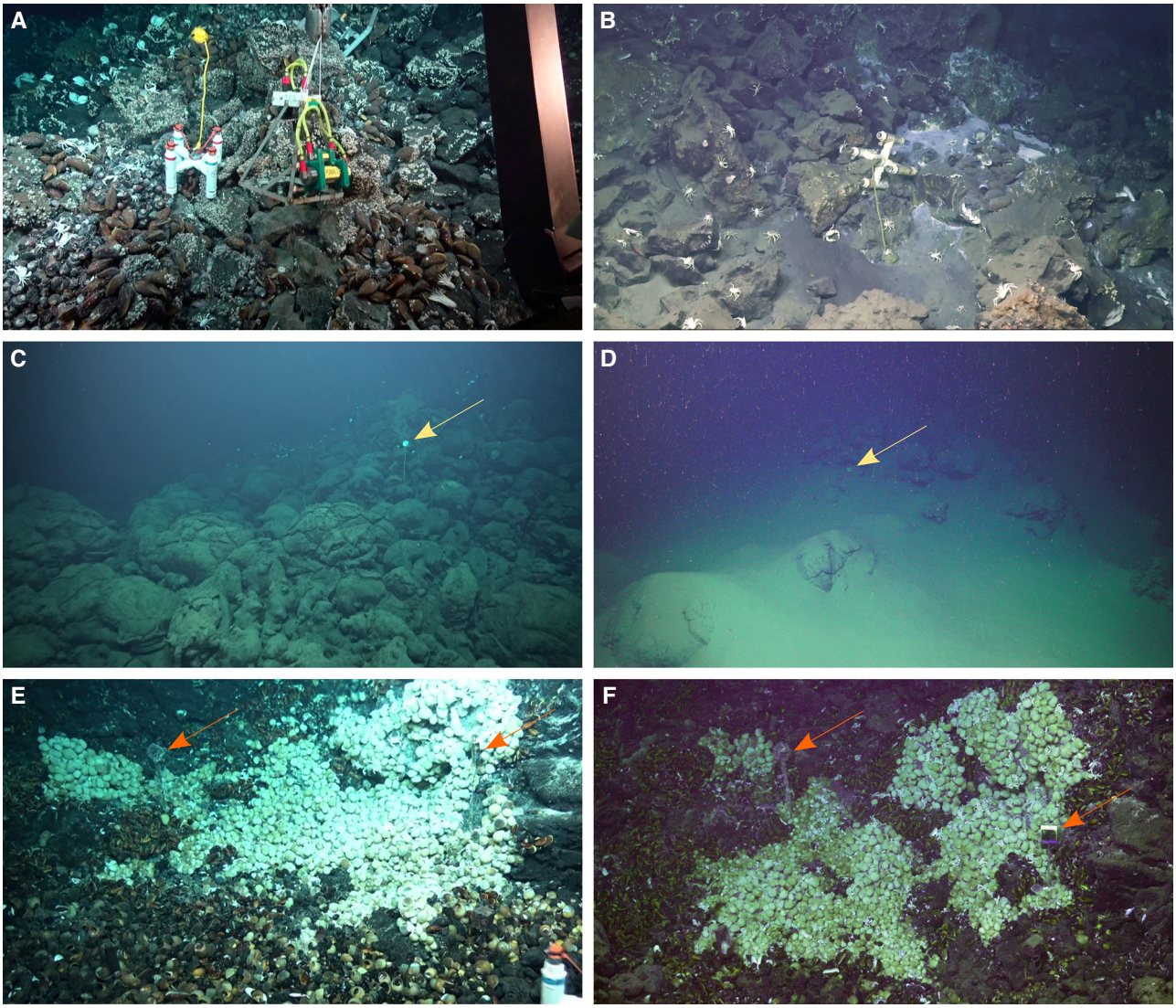

Fig. 2 | Comparison of 2019 pre-eruption conditions and 2022 post-eruption conditions at specific seafloor locations. Left panels show pre-eruption conditions and the right panels show post-eruption conditions at active hydrothermal vent fields with maximal ash deposition, Tow Cam (**A**–**D**), and negligible ash deposition, Tu'i Malila (**E**, **F**). Comparative photographs of a larval collection device that was deployed in 2019 and then located again in 2022 (**A**, **B**) and a navigational marker (yellow arrows) (**C**, **D**) demonstrate the thick ash deposition at Tow Cam. Panels **E** and **F** show navigational markers at Tu'i Malila (orange arrows), a southern site with little detectable ash, among qualitatively similar communities of chemosymbiotic animals in both years, indicating little change in the communities since the eruption.

volcanic ash into the Lau Basin. This hypothesis is supported by the severance and burial of two seafloor fiber-optic telecommunications cables to the south and southeast by ~30 m of ash[30]. Ongoing physical and geochemical analyses suggest that fast travelling SDCs are the primary mechanism that transported this massive volume of volcanic ash >80 km to the Lau Basin.

The impact of the Hunga volcanic eruption on Lau Basin hydrothermal vent communities

Regardless of its mode of arrival, the ash sedimentation observed here caused substantial changes in benthic megafaunal density and community composition at the active vent fields previously known to harbor abundant hydrothermal-vent associated animal communities[31,32]. Here, we performed a comparison of animal abundances before and after the eruption by examining ROV video footage from dives at three active vent fields (Tow Cam, ABE, and Tu'i Malila) on the 2019 CHUBACARC expedition and from our own 2022 expedition that spanned a range of ash depth (Fig. 3). Prior to the eruption, all three vent fields were dominated by large populations of IUCN-designated endangered or vulnerable species of chemosymbiotic molluscs (snails *Alviniconcha boucheti, Alviniconcha kojimai, Alviniconcha strummeri*, and *Ifremeria nautilei*, and mussel *Bathymodiolus septemdierum*), which obtain their primary nutrition from chemosynthetic bacterial symbionts hosted in their gills[31–33]. These vent fields were also previously inhabited by non-symbiotic heterotrophic grazers, filter-feeders, scavengers, and predators such as alvinellid worms (Fig. S4), anemones (Figs. S5, S6), stalked and acorn barnacles (Fig. S7), scale worms (Fig. S8), shrimp (Figs. S9, S10), squat lobsters (Fig. S11), true crabs (Fig. S12), whelks (Fig. S13), zoanthids (Fig. S14), and eelpout fishes[31–36]. After the eruption, the active vent field with the greatest ash deposition, Tow Cam, was almost completely devoid of the chemosymbiotic animals (Figs. 3a and 4). Living *Alviniconcha* snails were no longer present, while very small numbers of the snail *I. nautilei* and slightly more of the mussel *B. septemdierum* were observed (Fig. 3a). Instead, there were mainly large areas of empty snail and mussel shells (Fig. 4B–D; Supplementary Videos 1–3). At this site, we observed vigorously flowing high-temperature hydrothermal chimneys (Supplementary Video 4) and ash-covered low-temperature diffuse venting

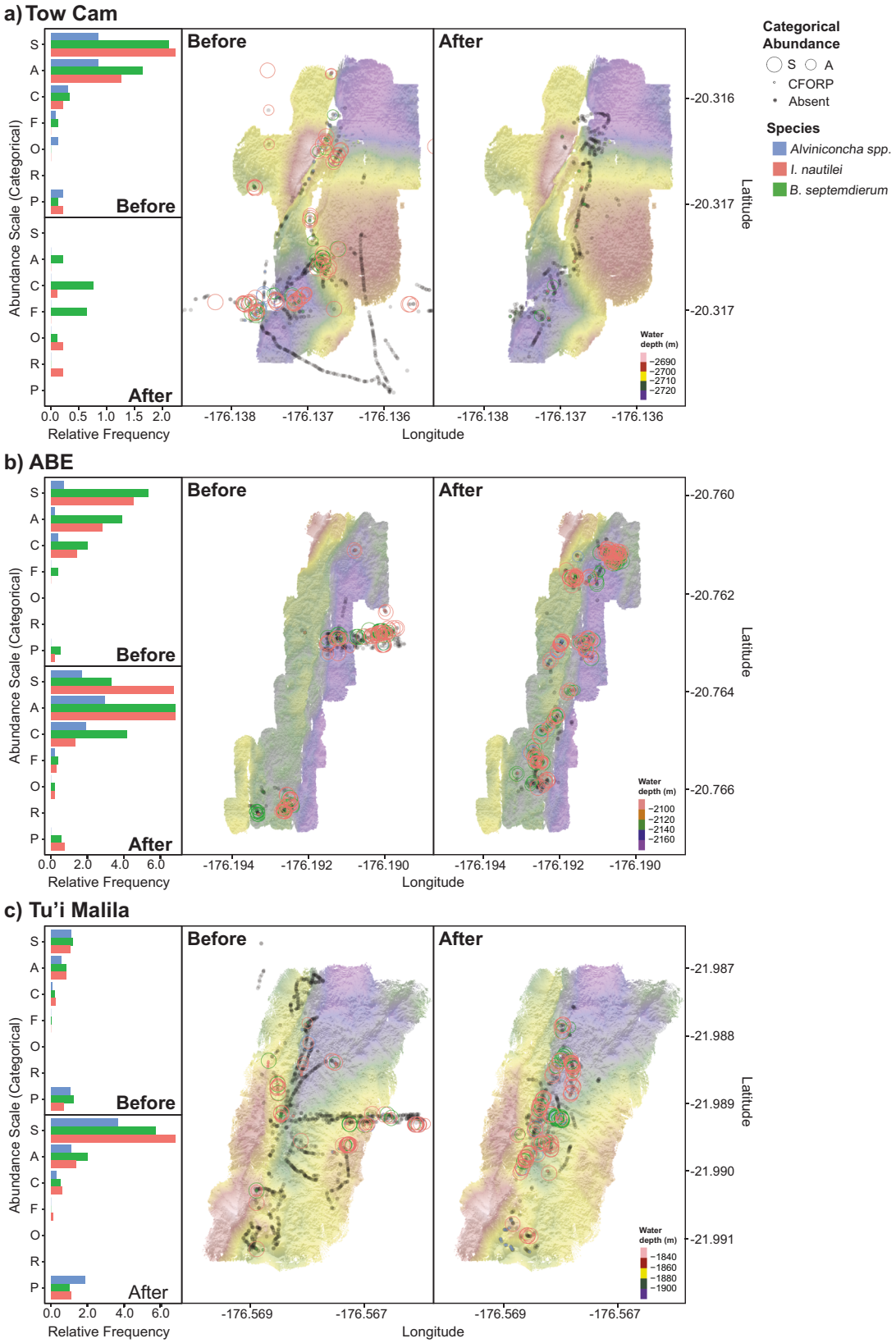

Fig. 3 | Categorical abundances of the foundation chemosymbiotic molluscs pre- and post-eruption at three hydrothermal vent fields with differing ash thicknesses. *Alviniconcha* spp. snails (blue), *Ifremeria nautilei* snails (red), and *Bathymodiolus septemdierum* mussels (green) at **a** Tow Cam, **b** ABE, and **c** Tu'i Malila vent fields before (2019) the Hunga volcanic eruption and after (2022). The categories Superabundant (S) and Abundant (A) are shown as differently sized open circles, while Common, Frequent, Occasional, Rare, and Present (CFORP) are all shown as an open smaller circle. Filled gray circles represent when the species were absent. Bathymetric data used to generate this figure was collected on the 2016 R/V Falkor (Schmidt Ocean Institute) cruise FK160407 and is publicly available through the Marine Geoscience Data System[82].

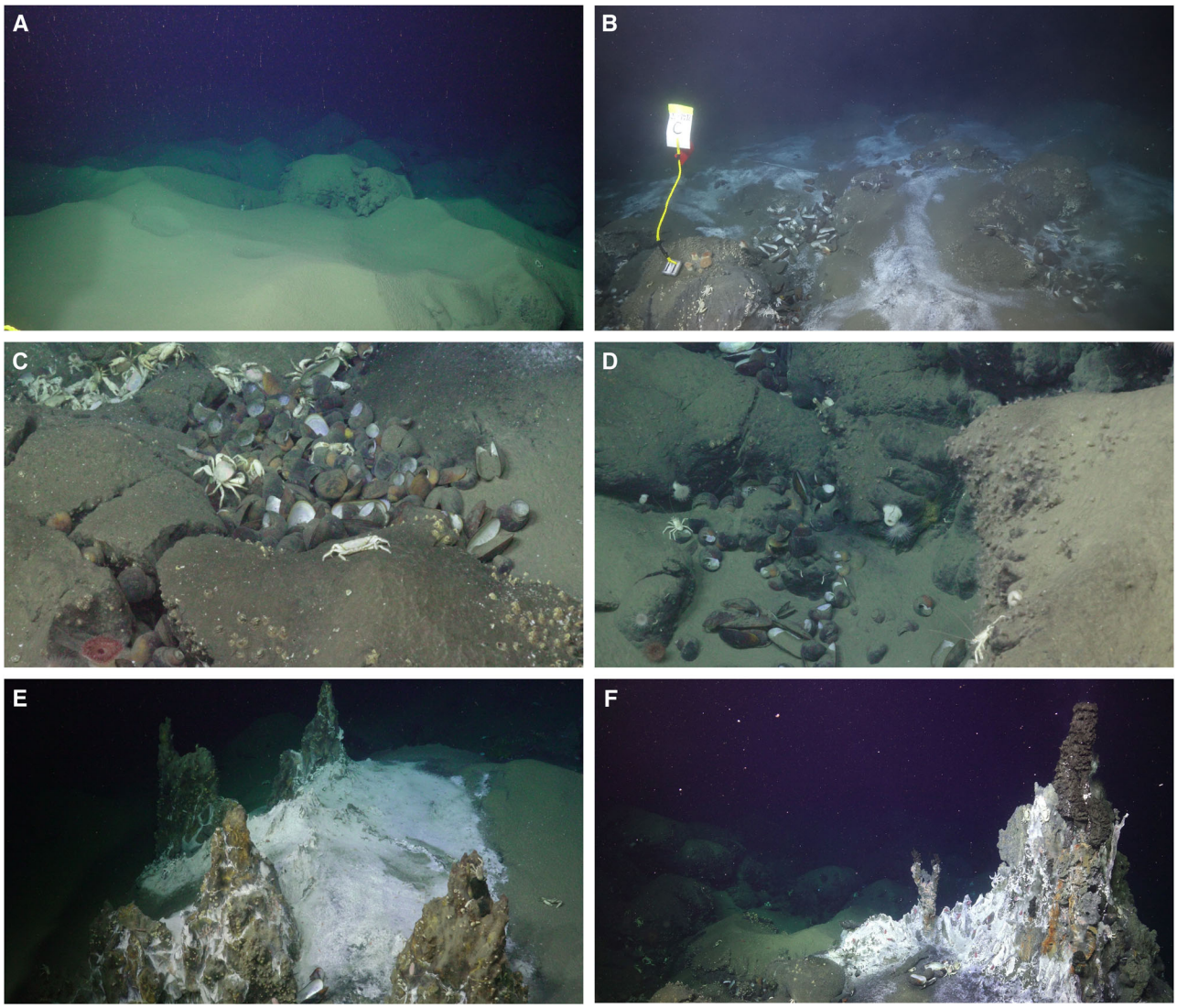

Fig. 4 | ROV photographs from Tow Cam, the vent field with the greatest ash thickness. A Thick ash deposits, **B** thick ash deposits with patches of empty shells and white microbial mat, likely sulfur-oxidizing bacteria. A new marker deployed on TN401 is also visible, **C**, **D** empty shells of dead chemosymbiotic snails and mussels among living crustaceans, anemones, and other grazers, scavengers, and filter feeders, **E**, **F** hydrothermal chimneys covered in white microbial mats and surrounded by ash deposits.

areas with obvious white microbial mat, likely sulfur-oxidizing bacteria (Fig. 4B, E, F; Supplementary Videos 1–3). Our observation of early colonization of bacterial mats on ash-covered diffuse flows is consistent with observations of bacterial mats dominating the earliest successional stages (<1 year) post-eruption at other hydrothermal vent sites that experienced catastrophic mortality of the dominant fauna[37,38]. The conspicuous megafauna that remained around diffuse venting and on chimneys were hydrothermal-vent associated heterotrophs: *Austinogrea* spp. crabs, *Munidopsis* spp. squat lobsters, *Vulcanolepas buckeridgeia* stalked barnacles, *Enigmaticolus desbruyeresi* whelks, and unidentified zoanthids (Figs. S4a–S14a). Though not decimated like those at Tow Cam, the chemosymbiotic animal communities were also drastically impacted at the ABE vent field (Fig. 3b), which was covered by up to 15 cm of ash. At Tahi Moana and ABE, we observed small patches of living *I. nautilei* snails and *B. septemdierum* mussels on chimneys and around diffuse flows (Figs. 3b, 5A; Supplementary Video 5), and even smaller numbers of large *Alviniconcha* spp. snails on chimneys at ABE only (Fig. 5B; Supplementary Video 6). As at Tow Cam, we observed normal populations of heterotrophs (Figs. S4b–S14b). Tu'i Malila did not have detectable ash deposition and had biological communities that were similar to pre-eruption communities (Figs. 3c, 6, S4c–S14c). Though we saw some changes in the relative frequency of abundance categories in the non-symbiotic, heterotrophic vent taxa between 2019 and 2022 at a given vent field, this variation did not relate to ash depth (Figs. S4–S14). For example, we more frequently observed Superabundant and Abundant categories for *Rimicaris* shrimp at Tow Cam after the eruption than prior, but also saw this same pattern at Tu'i Malila (Fig. S10). Overall, we did not observe a clear response to the eruption in the populations of heterotrophs.

Rapid sedimentation likely caused mass mortality due to oxygen deficiency

Rapid sedimentation events are known to cause major changes in benthic animal abundance and taxonomic composition due to differential survival in suspended sediment or variable escape from burial[39,40]. For mobile epibenthic organisms, survival after burial depends on vertical migration to the sediment surface, which is a function of sediment depth and animal motility[41–46]. Epibenthic bivalves and gastropods, like the chemosymbiotic mussels and snails here, are known to have varying responses to burial but, in general, have limited escape potential, especially in deep and dense sediments[42,47,48]. Sizeable respiratory effects and an associated decline in

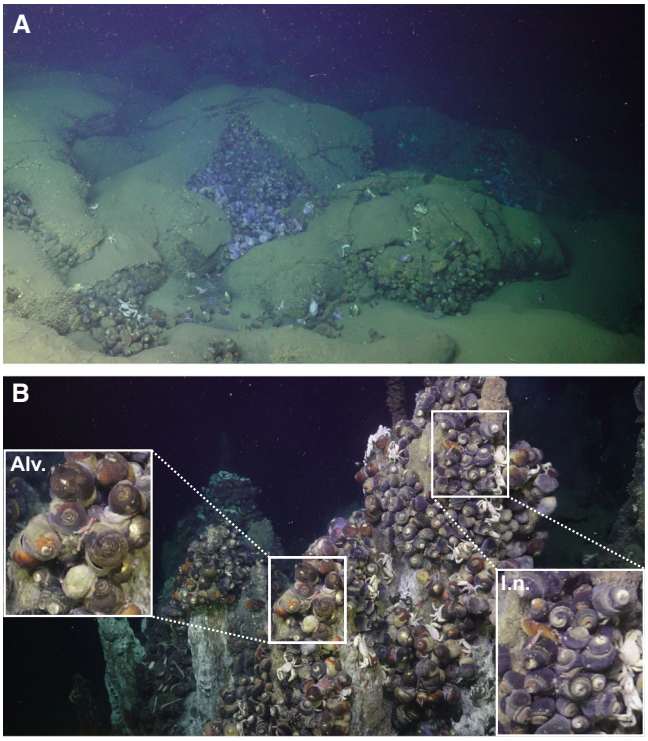

Fig. 5 | ROV photographs of patches of living chemosymbiotic molluscs among ash deposits at Tahi Moana and ABE. A Patches of living chemosymbiotic *I. nautilei* snails and *B. septemdierum* mussels among the ash deposits at the Tahi Moana vent field and **B**) *Alviniconcha* spp. and *I. nautilei* snails on a hydrothermal vent chimney at the ABE vent field. Inset boxes highlight representative patches of *Alviniconcha* spp. (Alv.) and *I. nautilei* (I.n.) snails.

health conditions have also been documented in shallow-water mussels subjected to suspended ash particles in the water column[49]. Without escape, mortality increases with sediment thickness and duration of burial, temperature, and increasingly finer-grained sediments, suggesting that oxygen deficiency is the ultimate cause of death, since these factors influence access to oxygen or respiratory rates[47,48]. Vent invertebrates hosting chemosynthetic symbionts have a very high oxygen demand to meet the metabolic demands of their chemoautotrophic symbionts[50]. Thus, they may be especially vulnerable to oxygen deficiency during ash burial or even when exposed to suspended ash particles. The observation that *Alviniconcha* snails were more impacted than *I. nautilei* snails or *B. septemdierum* mussels is consistent with this hypothesis, as *Alviniconcha* has the highest mass-specific respiratory rate[51]. The unburied or lightly sedimented patches of empty shells at the bases of chimneys and in some diffuse flow areas—which we interpret as derived from animals that had fallen from the vertical chimney surfaces onto the sediment surface or where vigorous fluid discharge may have pushed some sediment away—suggest that some chemosymbiotic snails and mussels avoided burial but still experienced substantial stress, and ultimately mortality, during this sedimentation event. Alternatively, these animals may have died due to prolonged stress associated with symbiont loss, but we do not consider this a likely cause of the widespread mortality of chemosymbiotic organisms. We observed that surviving chemosymbiotic snails and mussels at heavily-ashed sites had gill coloration similar to those at sites with little to no ash, suggesting normal symbiont density. Furthermore, *Bathymodiolus* mussels that have lost their symbionts have been shown to survive for months unfed[52], which is consistent with the general observation that molluscs can commonly survive prolonged periods of starvation[53–56]. Thus, it is unlikely that symbiont loss and subsequent starvation alone caused the mass mortality observed here.

The endurance of anemones and zoanthids (Figs. S5, S6, S14), crustaceans (Figs. S7, S9–S12), polychaete worms (Figs. S4, S8), and whelks (Fig. S13) suggests that these organisms had greater resilience to sedimentation, either through escape or survival. Anemones have been previously documented to be reasonably resilient to burial, likely due to their ability to withstand hypoxia and ability to emerge from burial[57]. As sessile filter feeders, barnacles are typically sensitive to sedimentation[58], though here they inhabited more vertical surfaces where sediment accumulation was relatively low. Similarly, the scale worms and alvinellid worms are also typically found on vertical chimney surfaces, where ash deposition was relatively minimal. Their survival could also have been facilitated by physiological adaptations, like specialized hemoglobins, that allow them to normally persist in chronic hypoxia[59]. In experiments, mobile crustaceans like the crabs, shrimp, and squat lobsters observed here, show relatively good resilience to sedimentation stress and burial, mostly due to their ability to quickly move vertically through the sediment[46], though the mass mortality of crustaceans buried in ash in the fossil record has been attributed to respiratory distress, based on mouth position[9,10,14,17].

Recovery of hydrothermal vent communities after ash deposition is unknown

Mass mortality of hydrothermal vent animals due to the underwater expulsion of volcanic lava has been observed occasionally[38,60,61] at areas of frequent tectonic and volcanic activity along active plate margins and seamounts. The dense chemosynthesis-based communities typical of these ecosystems are thought to experience recurrent natural disturbances varying in magnitude from total eradication caused by chemical and physical effects of submarine eruptions[62] to milder perturbations caused by temporal changes in the concentration of the chemosynthetic reductant hydrogen sulfide in venting fluid[63,64]. However, previous observation of the natural disturbances experienced by deep-sea hydrothermal vent communities has been exclusively limited to effusive seafloor eruptions that catastrophically paved over these habitats with solidified lava at vents along the Eastern Pacific Rise[60] and Juan de Fuca Ridge[37,61]. In these settings, the return to a near pre-eruption state occurred within only about 8 years through recolonization by planktonic larvae coming from both near and far sites[62,65–68]. Similar studies of community recovery on lava-covered volcanic flanks in shallow water suggest much longer recovery times in arctic ecosystems[69] and both slow and rapid succession in tropical reef communities[3,70–72]. Our understanding of the response of vent communities to natural disturbance is biased by a limitation of prior observations to fast-spreading ridges with a relatively frequent, decadal tempo of disturbance[38,61]. However, results from fast-spreading ridges cannot necessarily be extrapolated to other volcanic systems. For example, hydrothermal vents in back-arc basins, like those observed here, are thought to experience a much slower pace of natural disturbance and have shown remarkable ecological stability at the decadal scale[34,73], though models incorporating larval dispersal and population dynamics have predicted that vent communities in the Lau Basin could recover from a disturbance in under 5 years[74].

In a sedimentation disturbance event, community recovery could potentially occur through vertical migration through sediments after burial, lateral migration of adults or juveniles from nearby habitats, or recolonization through larval dispersal and settlement. Given that the vent fields are separated by distances too far for lateral migration by adults (9–212 km), recolonization via larval supply from distant vents is likely the major pathway for recovery for the decimated communities at Tow Cam, though the very small number of surviving *I. nautilei* snails and *B. septemdierum* mussels could also potentially act as a local source of larvae to this site. The remnant populations that persisted at the other vent fields are likely to also be important for recovery[75], especially for *Alviniconcha* snails. However, the change in substratum type, from exposed basaltic and andesitic to a heavily sedimented seafloor, may inhibit or prevent recolonization by these hard-bottom species even when larvae arrive from the local or regional pool.

Further observations of the vent fields impacted by the Hunga Volcano eruption have the potential to expand our knowledge of natural disturbance in vent ecosystems, successional processes, and the mechanisms by which such systems recover. The ash deposition we observed is a very different

kind of disturbance than the magmatic deposition events where succession has been studied elsewhere. Moreover, the linear gradient in ash disturbance intensity along this back-arc basin offers an unparalleled opportunity to follow the recovery of vent communities that have been differentially impacted by a single disturbance event. Such observations will yield important insights into the resiliency of deep-sea chemosynthetic ecosystems in general, including those impacted by sedimentation associated with deep-sea mineral extraction[76].

Methods

Remotely-operated vehicle dives

Thirteen dives with remotely-operated vehicle (ROV) *Jason II* (National Deep Submergence Facility, Woods Hole Oceanographic Institution) were conducted April 3–27, 2022 during cruise TN401 aboard the R/V *Thomas G. Thompson* (University of Washington). Five active and one inactive hydrothermal vent fields, at depths, ranging from ~1800 to ~2800 m, along the Eastern Lau Spreading Center-Valu Fa Ridge, were each visited on 1–3 separate dives. Total dive time at each vent field, including 1–1.5 h ascent and descent times, ranged from ~14 to ~52 h (Table S1).

Ash thickness, ash collection, and componentry and grain size analysis of collected ash

Ash thickness was measured by using a 61-cm metal probe marked in 7.6 cm increments along its length that was held by the ROV manipulator arm and pushed into the sediment until it hit seafloor rock below (Supplementary Video 7). Bagged ash samples consisted of 25 kg collected by scooping with canvas bags from 7 locations (Table S3). Particle size distribution was carried out by wet and dry sieving. Bulk representative 5 g splits from each location were wet sieved in half phi intervals down to 63 μm. A dilute concentration of Calgon ($Na_6O_{18}P_6$) and DI water was used to limit aggregating fine particles (<63 μm). Each size fraction was then dried in an oven at ~100 °C for 24 h to remove adsorbed water. Samples were then dry sieved to ensure the accuracy of the wet sieve process. Care was taken to avoid fine particle loss through dust clouds formed during the sieving process. Mass fraction was provided as a function of an equivalent diameter assuming spherical shape in whole ϕ bins, where $\phi = \log_2$(diameter in mm), from −2 to >5 (i.e., <0.032 to 4 mm).

Representative splits of ~200 particles per size fraction >0.125 mm at each sample site were analyzed for componentry under the optical microscope. Secondary scanning electron microscopy (SEM) in secondary electron mode was utilized to carry out the componentry of smaller particles. Each particle was categorized as one of three components: fresh volcanic glass, older volcanic, and foraminiferans. Fresh glass was visibly distinct from older pyroclasts based on micro-textural and angularity preservation. Fresh particles are highly angular and have a pronounced luster when compared to older pyroclasts (Fig. 1b). Limited physical evidence was visible to decipher sedimentary lithics from older pyroclasts. To limit human bias, lithic particles were categorized into older volcanics. Micro-textural analysis was continued under SEM.

Quantitative assessment of animal density and frequency

Observations of animal communities were quantitatively compared from video footage collected in 2022 from the ROV *Jason II*, and the most recent expedition that occurred prior to the eruption by the IFREMER ROV, *Victor 6000*, during CHUBACARC 2019[23]. High-definition video footage was converted to a single image frame per minute for analysis, and positioned in space using timestamped underwater tracking information obtained from each ROV system (*Jason II*: Sonardyne RangerPro USBL, Victor 6000: iXBlue POSIDONIA II). ROV dives that had spatial congruency for each site were selected for analysis, providing a total of seven dives from the *Jason II* and six dives from the *Victor 6000* (Table S4). The primary mission for these ROV dives was to undertake experiments and sample collections rather than conducting comparative habitat mapping surveys for each vent system. Hence, the ROV spent substantial time in certain areas rather than transecting systematically throughout the vent systems, introducing substantial spatial bias into the dataset. To address this and allow for comparisons between the 2019 and 2022 expeditions, image frames were spatially thinned by overlaying a 4 × 4 m polygon grid across each vent system, retaining a maximum of four images within each cell through random selection. Image frames containing no species, but where substrate was clearly visible were included, and all species were marked absent.

As scaling lasers were only enabled and clearly visible for an extremely limited subset of image frames, the visible surface area for each frame, defined as the area that was well-lit by the ROV, in focus and where all species were identifiable, was estimated using an organismal scaling approach (see Table S5 for preferential species and mean sizes used for scaling). Intact shells from dead target species were also used for scaling area estimations where appropriate to maximize the available dataset. Species of interest in the field of view and roughly perpendicular to the camera were measured using ImageJ[77], with pixels converted to distance units based on organism sizes obtained from samples taken during the 2022 expeditions or from literature sources (Table S5). Either the dimensions of the full image frame were determined, or the dimensions of a subset of the frame were used to constrain the usable field of view for area estimates. We estimated the abundance of 12 vent-associated organisms using a semi-quantitative categorical abundance approach, based on the SACFOR scale (Table S6), widely used for rapid assessment of marine habitats and species[78–80] but has not been applied to hydrothermal vent organisms. This approach allows for the rapid assessment of organismal abundance, and the scale used was based around six abundance categories, Superabundant, Abundant, Common, Frequent, Occasional and Rare, with a final criterion Present adopted for images where field of view scaling was not possible. The abundances that fall into each category were modified based on the body size class of the organisms studied, with 1–3 and 3–15 cm used in this study (Tables S4 and S5).

Data availability

Videos, photographs, and dive logs from cruise TN401 can be accessed through the National Deep Submergence Facility's publicly available archive at Woods Hole Oceanographic Institution.

Received: 15 February 2023; Accepted: 22 April 2024;
Published online: 13 May 2024

References

1. Crisafulli, C. M., Swanson, F. J., Halvorson, J. J. & Clarkson, B. D. Volcano ecology. In *The Encyclopedia of Volcanoes* (Elsevier Inc., 2015).
2. Vroom, P. S. & Zgliczynski, B. J. Effects of volcanic ash deposits on four functional groups of a coral reef. *Coral Reefs* **30**, 1025–1032 (2011).
3. Smallhorn-West, P. F. et al. Coral reef annihilation, persistence and recovery at Earth's youngest volcanic island. *Coral Reefs* **39**, 529–536 (2020).
4. Wu, C. C. et al. Pinatubo volcanic eruption exacerbated an abrupt coral mortality event in 1991 summer. *Geophys. Res. Lett.* **45**, 12,396–12,402 (2018).
5. Gallardo, V. A. & Castillo, J. G. Mass mortality in the benthic infauna of Port Foster resulting from the eruptions in Deception Island (South Shetland Is.). *Publnes Inst. Antart. Chil*. **16**, 1–13 (1968).
6. Lovell, L. L. & Trego, K. D. The epibenthic megafaunal and benthic infaunal invertebrates of Port Foster, Deception Island (South Shetland Islands, Antarctica). *Deep Sea Res. Part II* **50**, 1799–1819 (2003).
7. Jewett, S. C., Bodkin, J. L., Chenelot, H., Esslinger, G. G. & Hoberg, M. K. The nearshore benthic community of Kasatochi Island, one year after the 2008 volcanic eruption. *Arct. Antarct. Alp. Res.* **42**, 315–324 (2010).
8. Heikoop, J. M., Tsujita, C. J., Heikoop, C. E., Risk, M. J. & Dickin, A. P. Effects of volcanic ashfall recorded in ancient marine benthic

communities: comparison of a nearshore and an offshore environment. *Lethaia* **29**, 125–139 (1996).
9. Crawford, R. S. et al. Mass mortality of fossil decapods within the Monte León Formation (early Miocene), southern Argentina: victims of Andean volcanism. *Ann. Carnegie Mus.* **77**, 259–287 (2008).
10. Maguire, E. P., Feldmann, R. M., Casadio, S. & Schweitzer, C. E. Distal volcanic ash deposition as a cause for mass kills of marine invertebrates during the Miocene in Northern Patagonia, Argentina. *Palaios* **31**, 577–591 (2016).
11. Feldmann, R. M. et al. Formation of lobster-bearing concretions in the Late Cretaceous Bearpaw Shale, Montana, United States, in a complex geochemical environment. *Palaios* **27**, 842–856 (2012).
12. Palópolo, E. E. et al. An early Miocene spatangoid assemblage on a submarine volcanic ash dune from Patagonia (Argentina). *J. South Am. Earth Sci.* **108**, 103214 (2021).
13. Wall-Palmer, D. et al. Explosive volcanism as a cause for mass mortality of pteropods. *Mar. Geol.* **282**, 231–239 (2011).
14. Hyžný, M., Hudáčková, N. & Szalma, Š. Taphonomy and diversity of Middle Miocene decapod crustaceans from the Novohrad-Nógrad Basin, Slovakia, with remarks on palaeobiography. *Acta Geol. Slovaca* **7**, 139 (2015).
15. Gaines, R. R., Briggs, D. E. G., Orr, P. J. & Van Roy, P. Preservation of giant anomalocaridids in silica-chlorite concretions from the early Ordovician of Morocco. *Palaios* **27**, 317–325 (2012).
16. Orr, P. J., Briggs, D. E. G., Siveter, D. J. & Siveter, D. J. Three-dimensional preservation of a non-biomineralized arthropod in concretions in Silurian volcaniclastic rocks from Herefordshire, England. *J. Geol. Soc. Lond.* **157**, 173–186 (2000).
17. Maguire, E. P. *The Effect of Volcanic Ash Deposition on Marine Environments, Invertebrate Ecosystems and Fossil Preservation: Integrating Field Observations and Laboratory Experiments* (Kent State University, 2022).
18. Narbonne, G. M. THE EDIACARA BIOTA: Neoproterozoic origin of animals and their ecosystems. *Annu. Rev. Earth Planet. Sci.* **33**, 421–442 (2004).
19. Carr, J. L., Horváth, Á., Wu, D. L. & Friberg, M. D. Stereo plume height and motion retrievals for the record-setting Hunga Tonga-Hunga Ha'apai eruption of 15 January 2022. *Geophys. Res. Lett.* **49**, 1–7 (2022).
20. Proud, S. R., Prata, A. T. & Schmauß, S. The January 2022 eruption of Hunga Tonga-Hunga Ha'apai volcano reached the mesosphere. *Science (1979)* **378**, 554–557 (2022).
21. Seabrook, S. et al. Volcaniclastic density currents explain widespread and diverse seafloor impacts of the 2022 Hunga Volcano eruption. *Nat. Commun.* **14**, 7881 (2023).
22. Clare, M. A. et al. Fast and destructive density currents created by ocean-entering volcanic eruptions. *Science (1979)* **381**, 1085–1092 (2023).
23. Hourdez, S. & Jollivet, D. Chubacarc Cruise, RV L'Atalante. https://doi.org/10.17600/18001111 (2019).
24. Ferrini, V. L., Tivey, M. K., Carbotte, S. M., Martinez, F. & Roman, C. Variable morphologic expression of volcanic, tectonic, and hydrothermal processes at six hydrothermal vent fields in the Lau back-arc basin. *Geochem. Geophys. Geosyst.* **9**, Q07022 (2008).
25. Global Volcanism Program. Report on Hunga Tonga-Hunga Ha'apai (Tonga). In *Bulletin of the Global Volcanism Network* (eds. Bennis, K. L. & Venzke, E.) vol. 47 (Smithsonian Institution, 2022).
26. Manville, V. & Wilson, C. J. N. Vertical density currents: a review of their potential role in the deposition and interpretation of deep-sea ash layers. *J. Geol. Soc. London* **161**, 947–958 (2004).
27. Wiesner, M. G., Wang, Y. & Zheng, L. Fallout of volcanic ash to the deep South China Sea induced by the 1991 eruption of Mount Pinatubo (Philippines). *Geology* **23**, 885–888 (1995).
28. Carey, S. Influence of convective sedimentation on the formation of widespread tephra fall layers in the deep sea. *Geology* **25**, 839–842 (1997).
29. Wei-Haas, M. Tonga's strange volcanic eruption was even more massive than we knew. *Natl Geogr.* https://www.nationalgeographic.com/science/article/tonga-volcano-largest-eruption-pacific-ocean-tallest-plume (2022).
30. Rowley, J. Tonga eruption confirmed as largest ever recorded. https://niwa.co.nz/news/tonga-eruption-confirmed-as-largest-ever-recorded (2022).
31. Podowski, E. L., Ma, S., Luther, G. W., Wardrop, D. & Fisher, C. R. Biotic and abiotic factors affecting distributions of megafauna in diffuse flow on andesite and basalt along the Eastern Lau Spreading Center, Tonga. *Mar. Ecol. Prog. Ser.* **418**, 25–45 (2010).
32. Podowski, E. L., Moore, T. S., Zelnio, K. A., Luther, G. W. & Fisher, C. R. Distribution of diffuse flow megafauna in two sites on the Eastern Lau Spreading Center, Tonga. *Deep Sea Res. 1 Oceanogr. Res. Pap.* **56**, 2041–2056 (2009).
33. Tivey, M. K. et al. Links from Mantle to Microbe at the Lau Integrated Study Site. *Oceanography* **25**, 62–77 (2012).
34. Sen, A. et al. Community succession in hydrothermal vent habitats of the Eastern Lau Spreading Center and Valu Fa Ridge, Tonga. *Limnol. Oceanogr.* **59**, 1510–1528 (2014).
35. Soto, K. J. & Kim, S. Hydrothermal vent periphery invertebrate community habitat preferences of the Lau Basin. *J. Exp. Mar. Biol. Ecol.* **552**, 151741 (2022).
36. Kim, S. & Hammerstrom, K. Hydrothermal vent community zonation along environmental gradients at the Lau back-arc spreading center. *Deep Sea Res. Part I: Oceanogr. Res. Pap.* **62**, 10–19 (2012).
37. Marcus, J., Tunnicliffe, V. & Butterfield, D. A. Post-eruption succession of macrofaunal communities at diffuse flow hydrothermal vents on Axial Volcano, Juan de Fuca Ridge, Northeast Pacific. *Deep Sea Res. Part II: Top. Stud. Oceanogr.* **56**, 1586–1598 (2009).
38. Shank, T. M. et al. Temporal and spatial patterns of biological community development at nascent deep-sea hydrothermal vents (9°50'N, East Pacific Rise). *Deep Sea Res. 2 Top. Stud. Oceanogr.* **45**, 465–515 (1998).
39. Bigham, K. T., Rowden, A. A., Leduc, D. & Bowden, D. A. Review and syntheses: Impacts of turbidity flows on deep-sea benthic communities. *Biogeosciences* **18**, 1893–1908 (2021).
40. Bolam, S. G. Impacts of dredged material disposal on macrobenthic invertebrate communities: a comparison of structural and functional (secondary production) changes at disposal sites around England and Wales. *Mar. Pollut. Bull.* **64**, 2199–2210 (2012).
41. Hutchison, Z. L. et al. Survival strategies and molecular responses of two marine mussels to gradual burial by sediment. *J. Exp. Mar. Biol. Ecol.* **527**, 151364 (2020).
42. Kranz, P. M. The Anastrophic Burial of Bivalves and its Paleoecological Significance. *J. Geol.* **82**, 237–265 (1974).
43. Bolam, S. G. Burial survival of benthic macrofauna following deposition of simulated dredged material. *Environ. Monit. Assess.* **181**, 13–27 (2011).
44. Powell-Jennings, C. & Callaway, R. The invasive, non-native slipper limpet *Crepidula fornicata* is poorly adapted to sediment burial. *Mar. Pollut. Bull* **130**, 95–104 (2018).
45. Hinchey, E. K., Schaffner, L. C., Hoar, C. C., Vogt, B. W. & Batte, L. P. Responses of estuarine benthic invertebrates to sediment burial: The importance of mobility and adaptation. *Hydrobiologia* **556**, 85–98 (2006).
46. Maurer, D., Keck, R. T., Tinsman, J. C. & Leathem, W. A. Vertical migration and mortality of benthos in dredged material: Part II-crustacea. *Mar Environ Res* **5**, 301–317 (1981).
47. Chandrasekara, W. U. & Frid, C. L. J. A laboratory assessment of the survival and vertical movement of two epibenthic gastropod species, *Hydrobia ulvae* (Pennant) and *Littorina littorea* (Linnaeus), after burial in sediment. *J. Exp. Mar. Biol. Ecol* **221**, 191–207 (1998).
48. Hutchison, Z. L., Hendrick, V. J., Burrows, M. T., Wilson, B. & Last, K. S. Buried alive: The behavioural response of the mussels, Modiolus

modiolus and *Mytilus edulis* to sudden burial by sediment. *PLoS ONE* **11**, e0151471 (2016).
49. Salas-Yanquin, L. P., Navarro, J. M., Pechenik, J. A., Montory, J. A. & Chaparro, O. R. Volcanic ash in the water column: physiological impact on the suspension-feeding bivalve *Mytilus chilensis*. *Mar. Pollut. Bull.* **127**, 342–351 (2018).
50. Childress, J. J. & Girguis, P. R. The metabolic demands of endosymbiotic chemoautotrophic metabolism on host physiological capacities. *J. Exp. Biol.* **214**, 312–325 (2011).
51. Henry, M. S., Childress, J. J. & Figueroa, D. Metabolic rates and thermal tolerances of chemoautotrophic symbioses from Lau Basin hydrothermal vents and their implications for species distributions. *Deep Sea Res. 1* **55**, 679–695 (2008).
52. Piquet, B., Le Panse, S., Lallier, F. H., Duperron, S. & Andersen, A. C. "There and back again"—ultrastructural changes in the gills of *Bathymodiolus* vent-mussels during symbiont loss: back to a regular filter-feeding epidermis. *Front. Mar. Sci.* **9**, 968331 (2022).
53. Dunphy, B. J., Wells, R. M. G. & Jeffs, A. G. Oxygen consumption and enzyme activity of the subtidal flat oyster (*Ostrea chilensis*) and intertidal Pacific oyster (*Crassostrea gigas*): responses to temperature and starvation. *N. Z. J. Mar. Freshw. Res.* **40**, 149–158 (2006).
54. Haider, F., Timm, S., Bruhns, T., Noor, M. N. & Sokolova, I. M. Effects of prolonged food limitation on energy metabolism and burrowing activity of an infaunal marine bivalve, *Mya arenaria*. *Comp. Biochem. Physiol. A Mol. Integr. Physiol* **250**, 110780 (2020).
55. Zhao, Q., Cheung, S. G., Shin, P. K. S. & Chiu, J. M. Y. Effects of starvation on the physiology and foraging behaviour of two subtidal nassariid scavengers. *J. Exp. Mar. Biol. Ecol.* **409**, 53–61 (2011).
56. Stenton-Dozey, J. M. E., Brown, A. C. & O'Riain, J. Effects of diet and starvation on feeding in the scavenging neogastropod *Bullia digitalis* (Dillwyn). *J. Exp. Mar. Biol. Ecol.* **186**, 117–132 (1995).
57. Hendrick, V. J., Hutchison, Z. L. & Last, K. S. Sediment burial intolerance of marine macroinvertebrates. *PLoS ONE* **11**, e0149114 (2016).
58. Fabricius, K. E. & Wolanski, E. Rapid smothering of coral reef organisms by muddy marine snow. *Estuar. Coast. Shelf Sci.* **50**, 115–120 (2000).
59. Hourdez, S. & Lallier, F. H. Adaptations to hypoxia in hydrothermal-vent and cold-seep invertebrates. In *Life in Extreme Environments* (ed. Amils, R., Ellis-Evans, C. & Hinghofer-Szalkay, H). 297–313 (Springer, 2007).
60. Embley, R. W. et al. Geological, chemical, and biological evidence for recent volcanism at 17.5°S: East Pacific Rise. *Earth Planet. Sci. Lett.* **163**, 131–147 (1998).
61. Tunnicliffe, V. et al. Biological colonization of new hydrothermal vents following an eruption on Juan de Fuca Ridge. *Deep Sea Res. 1 Oceanogr. Res. Pap.* **44**, 1627–1644 (1997).
62. Mullineaux, L. S., Adams, D. K., Mills, S. W. & Beaulieu, S. E. Larvae from afar colonize deep-sea hydrothermal vents after a catastrophic eruption. *Proc. Natl Acad. Sci. USA* **107**, 7829–7834 (2010).
63. Nees, H. A., Lutz, R. A., Shank, T. M. & Luther, G. W. Pre- and post-eruption diffuse flow variability among tubeworm habitats at 9°50′ north on the East Pacific Rise. *Deep Sea Res. Part II: Top. Stud. Oceanogr.* **56**, 1607–1615 (2009).
64. Nees, H. A. et al. Hydrothermal vent mussel habitat chemistry, pre- and post-eruption at 9°50′North on the East Pacific Rise. *J. Shellfish Res.* **27**, 169–175 (2008).
65. Gollner, S. et al. Differences in recovery between deep-sea hydrothermal vent and vent-proximate communities after a volcanic eruption. *Deep Sea Res. Part I: Oceanogr. Res. Pap.* **106**, 167–182 (2015).
66. Mullineaux, L. S. et al. Prolonged recovery time after eruptive disturbance of a deep-sea hydrothermal vent community: prolonged recovery of vent community. *Proc. R. Soc. B: Biol. Sci.* **287**, 0–7 (2020).
67. Dykman, L. N., Beaulieu, S. E., Mills, S. W., Solow, A. R. & Mullineaux, L. S. Functional traits provide new insight into recovery and succession at deep-sea hydrothermal vents. *Ecology* **102**, 1–13 (2021).
68. Lutz, R. A. et al. Rapid growth at deep-sea vents. *Nature* **371**, 663–664 (1994).
69. Gulliksen, B. et al. in *The Marine Sublittoral Fauna of Jan Mayen Island BT—Jan Mayen Island in Scientific Focus* (ed. Skreslet, S.) 159–171 (Springer, Netherlands, Dordrecht, 2004).
70. Grigg, R. W. & Maragos, J. E. Recolonization of hermatypic corals on submerged lava flows in Hawaii. *Ecology* **55**, 387–395 (1974).
71. Tomascik, T., van Woesik, R. & Mah, A. J. Rapid coral colonization of a recent lava flow following a volcanic eruption, Banda Islands, Indonesia. *Coral Reefs* **15**, 169–175 (1996).
72. Putts, M., Parrish, F. & Trusdell, F. Structure and development of Hawaiian deep-water coral communities on Mauna Loa lava flows. *Mar. Ecol. Prog. Ser.* **630**, 69–82 (2019).
73. Du Preez, C. & Fisher, C. R. Long-term stability of back-arc basin hydrothermal vents. *Front. Mar. Sci.* **5**, 1–10 (2018).
74. Suzuki, K., Yoshida, K., Watanabe, H. & Yamamoto, H. Mapping the resilience of chemosynthetic communities in hydrothermal vent fields. *Sci. Rep.* **8**, 1–8 (2018).
75. Gollner, S. et al. Animal community dynamics at senescent and active vents at the 9°N East Pacific Rise after a volcanic eruption. *Front. Mar. Sci.* **6**, 832 (2020).
76. Gollner, S. et al. Resilience of benthic deep-sea fauna to mining activities. *Mar. Environ. Res.* **129**, 76–101 (2017).
77. Schneider, C. A., Rasband, W. S. & Eliceiri, K. W. NIH Image to ImageJ: 25 years of image analysis. *Nat. Methods* **9**, 671–675 (2012).
78. Crisp, D. J. & Southward, A. J. The distribution of intertidal organisms along the coasts of the English Channel. *J. Mar. Biol. Assoc. U. K.* **37**, 157–203 (1958).
79. Hiscock, K. *In situ* survey of intertidal biotopes using abundance scales and checklists at exact locations (ACE surveys). Version 1 of 23 March 1998. In *Biological Monitoring of Marine Special Areas of Conservation: a Hand Book of Methods for Detecting Change* (ed. Davies, J., Baxter, J., Bradley, M., Connor, D., Khan, J., Murray, E., Sanderson, W., Turnbull, C. & Vincent M.) Part **2**, (Joint Nature Conservation Committee, 1998).
80. Strong, J. A. & Johnson, M. Converting SACFOR data for statistical analysis: validation, demonstration and further possibilities. *Mar. Biodivers. Rec.* **13**, 2 (2020).
81. Wessel, P. et al. The generic mapping tools version 6. *Geochem. Geophys. Geosyst.* **20**, 5556–5564 (2019).
82. Ferrini, V. & Huang, S. Processed gridded near-bottom bathymetry data from the Lau Back-arc Basin acquired with ROV ROPOS during R/V Falkor expedition FK160407. *Marine Geoscience Data System*. https://doi.org/10.1594/IEDA/324649 (2016).

Acknowledgements

We are very grateful to the Kingdom of Tonga for permission to work in their waters. We thank the crews of ROV *Jason II* and the R/V *Thompson*. In addition, we thank T. Kula, K. Wishner, S. Gollner, S. Cronin, A. Soule, and K. Kelley for discussion and feedback related to our observations, and NSF REU student I. Yueh for assistance with ash thickness data. We thank undergraduate students A. Duffy, A. Smith, O. Reiber, and graduate student M. Lemke for their assistance with the analysis of ROV video data. We thank S. Hourdez and D. Jollivet for providing access to ROV footage from the 2019 CHUBACARC expedition. This work was supported by NSF awards OCE-1736932 (R.A.B.), OCE-1737382 (S.M.A), and OCE-1737145 (C.M.Y.), a University of Rhode Island 2023 First-Year Dean's Diversity Fellowship to J.M., and an NSF Graduate Research Fellowship award number 1747454 to M.A.H.

Author contributions

R.A.B., S.M.A., M.C., A.D. J.L., T.G., and C.M.Y. designed the study. R.A.B., M.C., S.M.A., D.D., V.J., T.B., J.B., S.B., M.B., L.B., A.C., E.J.C., M.A.H.,

M.H., T.M.L., C.Q.P., L.N.R., and A.T., and conducted video and ash thickness surveys via remotely operated vehicle. M.C. collected all ash samples, and M.C. and T.G. conducted all analyses on ash samples. J.M., J.L., and A.J.D. designed the post-cruise assessment of video footage and comparison to previous cruise footage with methods refinement by E.J.C., T.L., C.Q.P. and L.N.R., and M.B. Taxonomic guide for ROV surveys created by D.D. J.L., M.H., V.J., M.B., E.J.C., L.N.R., C.Q.P., J.M. performed the ROV footage observation and abundance estimations, and A.J.D. and J.M. did the associated analysis of resulting animal abundance data. R.A.B. and S.M.A. wrote the manuscript and all authors edited the manuscript.

Competing interests
The authors declare no competing interests.

Additional information
Supplementary information The online version contains supplementary material available at https://doi.org/10.1038/s43247-024-01411-w.

Correspondence and requests for materials should be addressed to Roxanne A. Beinart.

Peer review information *Communications Earth and Environment* thanks Alexander Liu, Evin Maguire and the other, anonymous, reviewer(s) for their contribution to the peer review of this work. Primary Handling Editors: Emma Nicholson and Joe Aslin. A peer review file is available.